Planetary and Space Science 224 (2022) 105597

Contents lists available at ScienceDirect

Planetary and Space Science

journal homepage: www.elsevier.com/locate/pss

Energetic electron lensing caused by Ganymede's magnetic field

M. Herceg [a,*], J.L. Jørgensen [a], J.M.G. Merayo [a], T. Denver [a], P.S. Jørgensen [a], M. Benn [a], S. Kotsiaros [a], J.E.P. Connerney [b,c], S.J. Bolton [d]

[a] Technical University of Denmark (DTU), Lyngby, Denmark
[b] Space Research Corporation, Annapolis, MD, United States
[c] NASA Goddard Space Flight Center, Greenbelt, MD, United States
[d] Southwest Research Institute, San Antonio, TX, USA

A B S T R A C T

The micro Advanced Stellar Compass (μASC) continuously monitors high energy particle fluxes in Jupiter's magnetosphere while providing attitude reference for the Juno Magnetic Field investigation. The μASC camera head unit (CHU) serves as a energetic particle sensor monitoring the radiation environment at Jupiter by sensing electrons greater than 15 MeV that pass through the CHU shielding. A comparison of the energetic electron population sampled during many orbits reveals events observed when Juno is traversing Ganymede's M-shell. We present observations of energetic electron depletions related to the interaction with Ganymede's magnetic field. The magnitude and extent of these depletions is associated with Juno's proximity to the magnetic field line passing through Ganymede. Analysis of the observations reveal that the charged particle depletion likely arises from electron scattering in Ganymede's magnetic field, observed within ~13° phase angle from the moon, beyond which the flux tubes refill due to diffusion.

1. Introduction

NASA's Juno spacecraft entered polar orbit about Jupiter on July 4th, 2016 (Bolton et al., 2017) and has now completed it primary mission of 36 orbits, systematically mapping the 3D magnetosphere of Jupiter (Bagenal et al., 2017). Located on the tip of the one of Juno's three solar arrays, the Magnetic Field Experiment, MAG (Connerney et al., 2017) includes the micro Advanced Stellar Compass (μASC), a magnetically clean attitude sensor designed and built at the Technical University of Denmark. In addition to its primary attitude determination function, the μASC is a star camera with a broad range of observational capabilities made possible by its versatile design. These include optical imaging of solar system bodies, autonomous detection and tracking of objects (Benn et al., 2017; Jorgensen et al., 2020) and detection of the high energy particles (e.g., Becker et al. (2017); Paranicas et al. (2017); Connerney et al., 2020). Electrons with energy >15 MeV, protons with energy >80 MeV and heavier elements with energy above ~100 MeV/nucleon penetrate the heavily shielded optical head of the Camera Head Unit (CHU) where they are detected by analysis of the CCD imagery (Becker et al., 2017); individual pixel counts are recorded in every telemetry packet sent to the spacecraft Command and Data Handling (C&DH) subsystem for eventual transmission to Earth.

μASC responds to >5 MeV electrons but with the highest efficiency at >15 MeV. However, the rapidly increasing differential fluxes with lower energy, may lead to sub-15 MeV fluxes having contributions to the μASC count-rate. The profile of the Ganymede-driven electron depletions shown in this work will reveal, amongst other results, which energies contribute to the ASC count-rate, at least at the M-shell of Ganymede. A wide spectrum of energetic particles are capable of penetrating the instrument shielding, but the star tracker signal is dominated by energetic electrons, with only ~0.1% of detections due to heavy ions. This data provides a continuous record of the in-situ energetic particle environment traversed by Juno and its interactions with the moons of Jupiter.

Juno regularly traverses M-shells of the Galilean moons during its polar orbit around Jupiter detecting variations in the energetic particle population associated with interactions between Jupiter's magnetosphere and the moons. M-shell is defined as the set of magnetic field lines that cross Jupiter's magnetic equator at Ganymede's radial distance from Jupiter. Similar to L-shell, which is calculated using the magnetic dipole (McIlwain, 1961), the M-shell is computed using additional contributions to the magnetic field, including higher degree spherical harmonics for the internal field and expressions accounting for the externally-generated field of the magnetodisc.

A number of authors have observed signatures of Jovian satellites in the energetic particle population for analysis of radial diffusion of trapped radiation (Simpson et al., 1974; Mogro-Campero and Fillius, 1974, 1976; Thomsen and Goertz, 1975; Thomsen, 1976; Mogro-Campero, 1976; Thomsen, 1977; Thomsen et al., 1977a, b). Dropout signatures

* Corresponding author.
E-mail address: mher@space.dtu.dk (M. Herceg).

https://doi.org/10.1016/j.pss.2022.105597
Received 16 May 2022; Received in revised form 17 October 2022; Accepted 31 October 2022
Available online 7 November 2022

(depletions) are generally observed due to losses on a moon's surface (Van Allen et al., 1980), but recent Juno observations at Europa's M-shell (e.g. Connerney et al., 2020; Allegrini et al., 2020) revealed a surprising enhancement of penetrating electrons. The particle signatures associated with Jupiter-moon interaction display characteristics unique to each moon, and are often heavily influenced by the magnetic longitudinal separation ("phase angle") between Juno and the moon magnetic footprint during transit. Since electrons can approach a moon, depending on their energy, both from its trailing (upstream) and from its leading (downstream) hemisphere (Thomsen and Van Allen, 1980 Liuzzo et al., 2020), depletions can form on both sides of the moon (leading/trailing). Therefore, while we can expect the deeper depletions at small absolute values of phase angle, that phase angle where losses are observed can be both positive and negative. We define positive phase angles as those where Juno is downstream of the moon with respect to the corotation flow of ambient magnetodisc plasma, while negative phase angles are configurations where for Juno trails the moon from its upstream hemisphere. The micro-signatures, caused by fresh wakes flux decreases in charged particle measurements (Paranicas and Cheng, 1997, Thomsen et al. 1977a,b, Selesnick, 1993; Roussos et al., 2007; Roussos et al., 2013), show small scale features and are strongly dependent on the phase angle, whereas macro signatures (the average effect that the satellite has on the distribution of trapped radiation) reflect a large scale features (Roussos et al., 2016; Van Allen et al., 1980).;

The motion of charged particles within the magnetic field of Jupiter is periodic and depends on particle energy, equatorial pitch angle (α) and the M-shell of the particle's guiding center. Trapped charged particles execute motion along particle's guiding center in three superimposed motions: gyro, bounce, and drift motion.

In this paper, we focus on signatures observed by Juno's μASC when Juno is traversing Ganymede's M-shell.To understand these signatures, we perform simulations for particle motion along field lines connecting the Juno spacecraft and Ganymede (Bonfond et al., 2013, 2017) (Fig. 1). Electron particle motion around Jupiter is governed by the three adiabatic invariants, gyration, bouncing and westward drift motion (Alfvén 1950; Northrop, 1966., Kruskal, 1958., Chew et al., 1955). The second adiabatic invariant, north-south particle bounce, is expressed as the latitudinal integral of the velocity parallel to the magnetic field, between the two mirror points for the trapped particle. If both the first and the second adiabatic invariants are conserved in the magnetic field, the particle will drift (the third adiabatic invariant) due to the radial gradient of the field (gradient drift) and the curvature of the magnetic field lines (curvature drift).

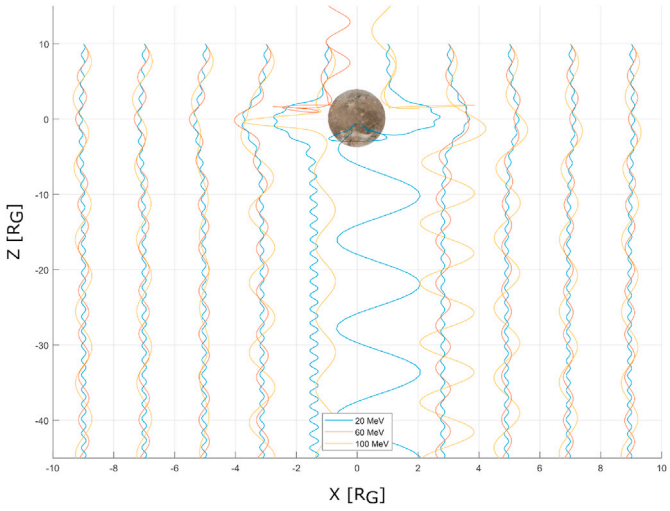

Fig. 1. Computed energetic particle trajectories (in a non-rotating Ganymede frame) passing by Ganymede illustrating a particle lensing effect of the moon illustrating 20, 60 and 100 MeV electron motion in a magnetic field computed using a Ganymede dipole and the Jovian magnetic field (JRM09 model).

A charged particle injected near Ganymede will be guided by the magnetic field of Jupiter (Connerney et al., 2018), the magnetodisc (Connerney et al., 2020) and the internal magnetic field of Ganymede (Kivelson et al., 1997, 2002). Particle trajectories were computed using the DTU particle simulation toolbox for the electrons with energies of 20, 60 and 100 MeV (Fig. 1). Verification of the DTU particle simulation toolbox was done by comparison with previously published simulated particle trajectories (Öztürk, 2012) and simulations reported in Liuzzo et al. (2020). Uncertainties in particle trajectory calculations are small (<5% in the gyration radius), dominated by the accumulation of errors in numerical integration and the fidelity of the magnetic models used. Since particle motion is simulated $15R_J$ away from Jupiter, the magnetic model uncertainties are minimal but for possible time variability of the magnetodisc (Caudal, 1986; Mauk et al., 1998, 2022). However, uncertainties in Ganymede's magnetospheric interaction fields (Kivelson et al., 2002) and those due to the interaction with Jupiter's field will directly impact simulated particle motions, and to a lesser extent, the total lensing effect.

Fig. 1 shows results for the motion of a cloud of particles with a range of energies. Simulation results may also be compared to the analytical expressions from Guio et al. (2020) and Thomsen and Van Allen (1980), where estimated particle parameters for 20, 60 and 100 MeV electrons injected at the equator with 30° pitch angle at the distance of 15 R_J are: drift period is 5.6 h, 1.9 h and 1.1 h; bounce period is 10 s, 10 s and 10 s; drift per bounce rate is 0.2°, 0.5°, 0.9°; and gyro radius is 464 km, 1370 km and 2275 km, respectively. These calculations show agreement with the simulations shown on Fig. 1.

If we assume rigid corotation, all charged particles will have an eastward drift equal to the Jupiter magnetic field rotation of $\omega_J = 36°/h$, while Ganymede orbits Jupiter at about $\omega_G = 2°/h$, meaning that the relative motion of charged particles due to corotation relative to Ganymede is 34°/h. This also corresponds to the Ganymede's magnetic footprint westward drift, which creates the wake region downstream of the moon (Fig. 2).

For estimating the energy dependent electron drift rate, we should subtract from this their westward drift around Jupiter. Since this westward drift increases with energy, there will be an energy at which the 34°/h is cancelled out. This energy (~10 MeV for Ganymede's orbit) is typically called the Keplerian resonant energy (E_K). Electrons with $E < E_K$ will approach Ganymede from the upstream direction or trailing hemisphere (similar to low energy corotating particles) and if absorbed, their wake will form in Ganymede's downstream (leading) hemisphere with respect to the corotation flow. At $E > E_K$ occurs the opposite, ie. the wake forms in Ganymede's (trailing) upstream hemisphere with respect to corotation flow. Using the drift velocity estimates of Guio et al. (2020) and assuming a 30° equatorial pitch angle, E_K is at ~10 MeV. If an 80% corotation is used, E_K drops to about 8 MeV. Liuzzo et al. (2020), using a different magnetic field model and assuming 80% corotation (Bagenal et al., 2016), estimate that E_K can be as low as ~2 MeV. For the follow-up discussion, we will base E_K based on the Guio et al. (2020) study, ie. at 8–10 MeV.

A 60 MeV electron with 30° pitch angle will have drift period of 1.9 h and will drift westward with velocity of $\omega_e = 190°/h$. Assuming rigid corotation, the drift velocity will be 156°/h (811 km/s) and drift per electron bounce would be 9954 km. This means that a 60 MeV electron would bounce ~0.5 times while crossing the width of Ganymede ($2R_{GA}$).

Part of the bounce trajectory of the 60 MeV electron (Fig. 1) was simulated using a model for Jupiter's field, JRM09 (Connerney et al., 2018), a magnetodisc model (Connerney et al., 2020), and a Ganymede magnetic dipole model (Kivelson et al., 2002) with coefficients [g10, g11, h11] = [-728, 66, −11] nT. Unlike the northward dipole moment of Jupiter, represented by the JRM09 model, Ganymede's magnetic moment points southward. The magnetic field due to JRM09 and magnetodisc at Ganymede (~15 R_J away from Jupiter)

is ~75 nT, almost 10% of Ganymede's equatorial magnetic field.

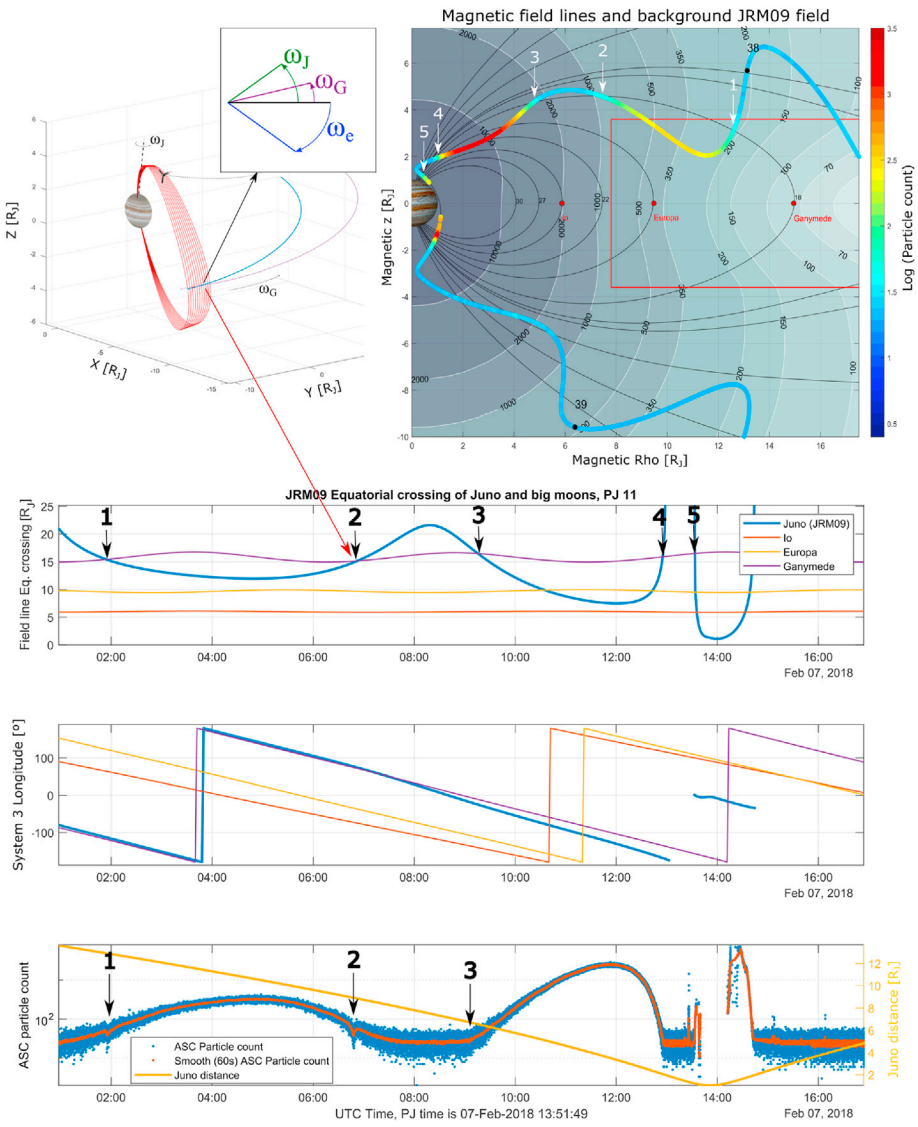

Fig. 2. Observed particle flux disturbance due to Ganymede. Left top panel illustrates the geometry during event #2 (including angular velocity directions of Jupiter, Ganymede and electrons), during which Juno's equatorial crossing point crosses Ganymede's; magnetic field lines (red) intersecting the Juno trajectory (black) and magnetic equator (blue). The top right panel shows Juno's trajectory in magnetic equatorial coordinates color coded with the intensity of radiation observed by the μASC. Bottom 3 panels show satellite and spacecraft equatorial crossing distance, S3 longitude, and μASC observations as a function of time (blue and red, averaged). The values of Juno's magnetic equatorial footprint (blue line on the first panel) reveals when it crosses the M shell of Ganymede's (purple line). Ganymede interaction events 1, 2, and 3 indicated.

Therefore, particle motion further away from Ganymede (>3 R_{GA}) will be governed primarily by the magnetic field of Jupiter and the magnetodisc since the contribution from Ganymede's magnetic field model becomes small in comparison.

The simulation shows that electrons with energies of 20–100 MeV passing within ~5 Ganymede radii (R_{GA}) may be redirected up to ~4 R_{GA} away from Ganymede, producing a lensing effect in the particle population of up to ~8 R_{GA} in width. This is mainly caused by strong magnetic field of Ganymede (Kivelson et al., 1996, Kivelson et al., 1997, Kivelson et al., 2002, Frank et al., 1997, Gurnet et al., 1996, Williams et al., 1997a, Williams et al., 1997b, Paranicas et al., 1999) which is guiding electrons that would normally impact Ganymede away from its surface. Particles injected directionally close to Ganymede polar regions will naturally enter the loss cone and will be absorbed by the surface of Ganymede.

During Juno's prime mission, the spacecraft crossed Ganymede's M-shell more than 120 times with the majority of crossings occurring when Ganymede was well separated from Juno in longitude (phase angle). A small number of crossings occurred with Juno and Ganymede in or near magnetic conjugacy, revealing a repeated signature of a lensing effect from Ganymede's magnetic field on high energy particles.

2. Observations

The Juno spacecraft experiences multiple traversals of Ganymede's M-shell on approach to Jupiter, a consequence of its polar orbit and the ~10-h rotation of Jupiter's magnetic field. These may occur at radial distances spanning Ganymede's orbital radius (14.96 R_J), their number and location largely determined by Juno's System III longitude on approach (Fig. 2, right panel). When Juno crosses an M-shell that intersects the orbit of one of Jupiter's moons, variations in the charged particle environment (Szalay et al., 2020), plasma waves (Sulaiman et al., 2020), radio emissions (Louis et al., 2020), and magnetic field (Gershman et al., 2019; Connerney et al., 2020; Allegrini et al., 2020) are observed associated with the moon's interaction with the Jovian magnetosphere. Juno's 11th orbit presented a particularly auspicious opportunity to observe Ganymede's interaction with the magnetosphere, with numerous traversals of Ganymede's M-shell occurring at small phase angle separation. Three of the traversals occurred while Juno and Ganymede were separated by a large radial distance (few to ~10 R_J) and within a few degrees of System III (1965) longitude. As shown in top left panel of Fig. 2, Juno's trajectory is illustrated with a black dashed line, and

magnetic field lines that Juno crosses during the second Ganymede M-shell traversal are colored in red. The magnetic equatorial crossing point of the field line intersecting the spacecraft trajectory is marked with a blue line, while the equatorial crossing point of the field line passing through Ganymede's orbit is colored in purple; both calculated using the JRM09 magnetic field model and the Connerney et al. (2020) magnetodisc model. Where the two cross, Juno is traversing Ganymede's M-shell.

An overview of orbit 11 appears in the top right panel of Fig. 2. Juno traverses Ganymede's M-shell 5 times while inbound. Another way to illustrate M-shell traversals appears in the second row of Fig. 2, which shows the radial distance to the equatorial crossing point of the Juno spacecraft and the Galilean satellites as a function of time. Similarly, the third row shows the variation in time of the System III longitude of Juno and the major moons. Where Juno's and Ganymede's curves intersect in the second and third panel, Juno is traversing Ganymede's M-shell and on, or near, the same magnetic field line as Ganymede. This alignment is observed by μASC three times during orbit 11 (crossings 1, 2 and 3 on bottom of Fig. 2).

Energetic particle omni-flux μASC observations (Fig. 2, bottom panel) show many features: a large, gradual increase in the particle population (between crossing 1 and 2) as Juno approaches the magnetic equator between the orbits of Ganymede and Europa; passage through the radiation belt at high magnetic latitudes (radiation belt horn) right after crossing 3 at a distance of a few R_J; passage through perijove and again crossing of the radiation belt horn while outbound, this time much closer to Jupiter where the radiation is most intense. Apart from these large and expected radiation signatures, there are several small disturbances, which Juno observes while it samples the distribution of MeV electrons in the radiation belts, in the auroral regions (Kotsiaros et al., 2019; Mauk et al., 2020), and episodic particle events mapping to very large radial distances. The signatures we are concerned with here are those observed prior to perijove (marked 1, 2, 3) that correspond to the predicted traversal of Ganymede's M-shell depicted in the second and the third panels. During the first traversal at around 01:55 UTC and radial distance of 13 R_J (Fig. 2), Juno's footprint meets the one of Ganymede with −5.5° S3 longitude separation (Ganymede's wake region). Then, Juno and Ganymede have the same equatorial crossing distance (where purple and blue line meet on the second row plot of Fig. 2). At nearly the same time a significant (~25%) decrease in energetic particle flux is observed by the μASC (bottom plot in Fig. 2). Similarly, at 06:47 UTC, Juno traverses Ganymede's M-shell even closer in phase (difference between the crossings S3 longitude is −2.5°) and observes a significant depletion (~50%) in particle flux, which is very similar to 40–50% reduction in flux reported by Allioux et al. (2013). The third traversal occurs at 09:05 UTC, but by then the Juno and Ganymede field lines are separated by ~13° S3 longitude resulting in a much weaker energetic particle depletion.

μASC observations displayed in the bottom plot of Fig. 2 show clear signatures of Ganymede's interaction with the charged particle environment. However, the signatures of the highly energetic particles that μASC is sensitive to (>15 MeV; Becker et al., 2017) are only observed when Ganymede and Juno have small phase separation (events 1, 2 and 3).

3. Results

Depletions of energetic electrons are observed when Juno crosses the drift shell of Ganymede at small phase angles, as summarized in Fig. 3. The location of the Ganymede's drift shell is estimated from the JRM09 (Connerney et al., 2018) and the magnetodisc (Connerney et al., 2020).

Events 1, 2 and 3 exhibit a similar spatial scale for all 3 events (Fig. 3), varying between 8.9 and 11.1 Ganymede radii (R_{GA}) in width. The time spent in the particle depletion region is dictated by the angle between Juno's and Ganymede's magnetic equator crossing footprints; if small the depletion persists longer. The width of the depletion region can be compared to the simulations to illustrate the Ganymede lensing effect (Fig. 1). The simulation shows a Ganymede magnetic lensing of ~8 R_{GA}, compared to the average observed width of ~10 R_{GA}. The small difference between model and observation could be due to other contributors to the measured particle flux, or temporal variation in the magnetic field, not captured by the models used for estimating Juno-Ganymede footprint crossing.

A depletion of ~15–50% in particle counts is observed with the magnitude of the depletion depending on phase angle, a reduction of 50% experienced at small (−2.5°) phase angle, and a 15% reduction at large (−13°) phase angle. Traversals of Ganymede's M-shell that occur with greater phase separation (>~13° S3 longitude) evidence no particle depletion.

If Ganymede were to be unmagnetized, the depletion region width D_G would be $D_G = 2 \bullet (R_G + 2 \bullet r_e)$; with R_{GA} being the Ganymede radius and r_e the energy dependent gyro radius of electrons, resulting in a

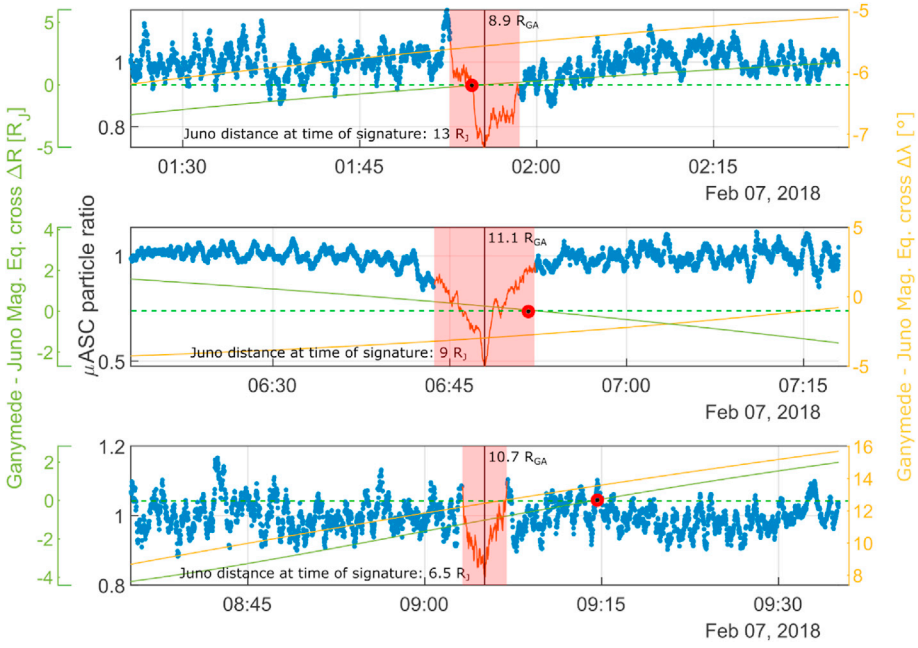

Fig. 3. μASC observations as a function of time (events 1, 2, 3, from top to bottom). The green line shows the difference in the radial distance (R_J) between the equatorial crossing point of field lines through Ganymede and Juno, and the yellow line shows angular difference. The dashed green line indicates where Juno's magnetic footprint meets Ganymede's M-shell (ΔR = 0). Red shaded area spans the Ganymede signature and the red filled circle indicates where the JRM09+magnetodisc model predicts the crossing of Juno and Ganymede M-shells.

broadening of the depletion region by $2*r_e$ on each side of the moon. Assuming that electrons contribute significantly to the observed depletion have an upper energy limit of 60 MeV (gyro radius of 1369 km and equatorial pitch angle of 30°), we calculate a depletion with total width of $D_G = 10750$ km *(~4 R_{GA})*. The theoretical depletion estimate of a 4 R_{GA} width for the unmagnetized Ganymede is much smaller than ~10 R_{GA} width observed by the μASC instrument. Width of this size can only be caused by the effective obstacle associated with Ganymede being larger than the moon alone. The best candidate making this obstacle larger is Ganymede's magnetic field, guiding electrons, that would normally hit Ganymede, away from its surface.

As previously discussed, a 60 MeV electron with 30° pitch angle would bounce ~0.5 times while crossing a width of Ganymede (2 R_{GA}), and ~2.5 times during the observed Ganymede crossing event with a width of ~10 R_{GA}. The electrons whose bouncing trajectories connect to Ganymede are scattered around Ganymede due to the lensing effect of Ganymede's magnetic field or absorbed by it. A flux tube connecting Jupiter and Ganymede is thus typically losing electrons from its population. Contrary to the ions, the fast electrons can bounce several times in Jupiter-Ganymede flux tube during the crossing time of the moon, further increasing electron depletion.

Multiple bounces will cause depletions in electron population detected up to 13° longitude away from Ganymede, where it will gradually be filled back in by particles diffusing radially into it from the neighboring reservoir of the ambient plasma. This happens due to a response to the fluctuation in the neighboring magnetic and electric fields, as suggested by Mead and Hess (1973) and Van Allen et al. (1980), and implies that electrons are not lost but refilled at distances >13° when they rejoin their original drift shell in the ambient magnetosphere. As deflected particles due to the magnetic lensing are populating the neighboring drift shells, an enhancement of particles population in these neighboring regions should be observed. However, due to a possible wide energy dispersion, this enhancement may be distributed over a relatively large area and possibly be reduced to the noise level of the μASC instrument. By collecting data from future Ganymede M-shell crossings, a more detailed "refill" rate can be defined. This can be a reason for smooth and not very deep depletions, which can then be refilled fast, only within ~13° separation from Ganymede, as Juno's μASC observations show. However, at distances >13° the signature is very weak and at the edge of μASC detection sensitivity, as in the plot for perijove 1 (Fig. 4). Stronger particle depletions are observed when Juno is trailing Ganymede. This can be explained by the wake flow and magnetospheric plasma not filling the Ganymede particle trail, compared to the plasma density in Ganymede's ram direction. Signatures might also originate from the wake region, if accounting for the bend back of the field due to radial currents and half bounce drift.

Thus far during Juno's prime mission, there have been more than 120 traversals of Ganymede's M-shell. Of these only a handful with small phase separation show clear signatures (Fig. 4) of Ganymede magnetic lensing. Our analysis, supported by the simulations of energetic electron motion in the environment of Ganymede, shows that the magnetic lensing of Ganymede combined with the effect of double loss cone absorption has a width of ~26,000 km, or ~9 Ganymede radii, which is much larger than A width of 4 R_{GA} for the estimated unmagnetized Ganymede case.

4. Conclusions

Comparison of the particle population model around Jupiter with individual perijove particle observations reveals up to 52% depletion in electron flux when Juno is traversing M-shell of Ganymede. Particle fluxes observed while traversing Ganymede M-shell are depend on the phase angle between Juno and Ganymede, since successive depletions in electrons are only observed up to 13° away in longitude, beyond which the particle gap is gradually filled by diffusion from the ambient plasma.

The μASC observations, supported by simulations of electron motion, show that the magnetic lensing of Ganymede combined with the effect of double loss cone absorption has a width of ~26,000 km, or ~9 Ganymede radii, which is 2.5 times wider than theoretical depletion estimate for the unmagnetized Ganymede. Width of this size is partially caused by Ganymede's magnetic field, guiding electrons, that would normally hit Ganymede, away from its surface. Additionally, the bouncing electrons in a flux tube connecting Jupiter and Ganymede are lost due to increased absorption in the double Jupiter-Ganymede loss cone.

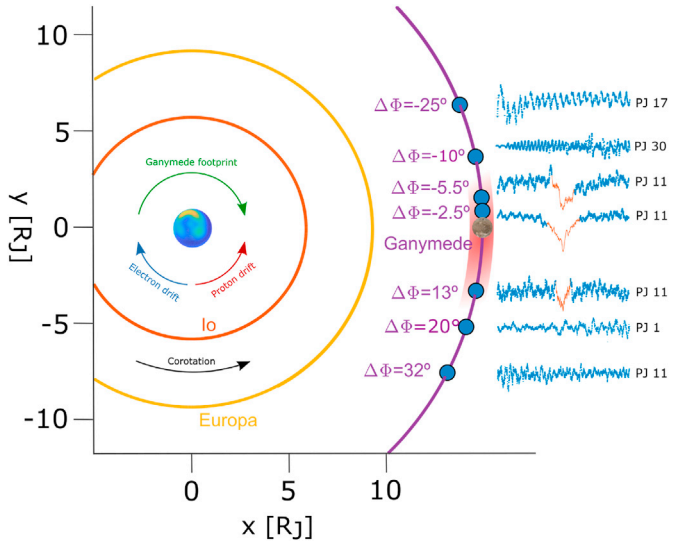

Fig. 4. Footprint of the Galilean moons in the magnetic equator and the associated depletion of the high energy particle population. Dots (blue filled circles) mark the S3 longitude of the equatorial crossing point of the field line through Juno as Juno transverses the Ganymede M-shell (shell composed of magnetic field lines of all magnetic longitudes). Shaded area shows how far away in S3 longitude the particle depletion is observed in the radiation data, illustrated (blue) to the right. Negative Δλ indicates when Juno footprint is trailing Ganymede (wake region).

Close agreement between Ganymede magnetic lensing simulation and μASC observations confirms that the JRM09 and magnetodisc model fits very well with observations and can be reliably used for magnetic field tracing and M-shell definition within the inner (<30 R_J) magnetosphere. This novel use of the μASC star tracker as an energetic particle detector is a useful complement to Juno's dedicated radiation monitoring instruments, extending detection capability to particle energies >15 MeV. The results of analysis of a high energy particle population in the near-Ganymede region within the Jovian magnetosphere can help determine capability of Ganymedes's magnetic field to protect future missions, and instruments on board, from the intense Jovian high energy flux.

Plain language summary

The μASC camera onboard Juno, serving primarily as an attitude reference for the magnetic field investigation, also continuously monitors high energy particle fluxes in Jupiter's magnetosphere. This paper presents observations of the energetic electron environment obtained as Juno crosses Ganymede's M-Shell, revealing particle flux depletions (up to 50%) associated with interactions with Ganymede's magnetic field.

Author statement

M. Herceg: Conceptualization, Methodology, Data curation, Writing-Original draft preparation, Visualization, Software, Validation, Reviewing and Editing, **J. L. Jørgensen:** Conceptualization, Methodology, Supervision.

J. M. G. Merayo: Software.

T. Denver: Software, Data curation.

P. S. Jørgensen: Supervision.

M. Benn: Software, Data curation, **S. Kotsiaros:** Reviewing and Editing, **J. E. P. Connerney:** Writing- Original draft preparation, Reviewing and Editing, Supervision.

S. J. Bolton: Reviewing and Editing.

Declaration of competing interest

The authors declare that they have no known competing financial interests or personal relationships that could have appeared to influence the work reported in this paper.

Data availability

https://zenodo.org/record/5503853#.Y00gtkxBy70

Acknowledgments

All authors acknowledge support from the Juno project. Data supporting the conclusions are available in the permanent archival data repository, Zenodo (Herceg et al., 2021), and will soon be archived in the NASA Planetary Data System at https://pds.nasa.gov.

References

Alfvén, It, 1950. Cosmical Electrodynamics. Clarendon Press, Oxford.

Allegrini, F., Gladstone, George, Hue, Vincent, Clark, G., Szalay, J., Kurth, William, Bagenal, F., Bolton, S., Connerney, J., Ebert, Robert, Greathouse, Thomas, Hospodarsky, G., Imai, M., Louarn, P., Mauk, B., Mccomas, David, Saur, J., Sulaiman, A., Valek, P., Wilson, R., 2020. First report of electron measurements during a Europa footprint tail crossing by Juno. Geophys. Res. Lett. 47. https://doi.org/10.1029/2020GL089732.

Allioux, R., Louarn, P., André, N., 2013. Model of energetic populations at Ganymede, implications for an orbiter. Adv. Space Res. 51 (7), 1204–1212. https://doi.org/10.1016/j.asr.2012.10.033. ISSN 0273-1177.

Bagenal, F., Wilson, R.J., Siler, S., Paterson, W.R., Kurth, W.S., 2016. Survey of Galileo plasma observations in Jupiter's plasma sheet. J. Geophys. Res. Planets 121. https://doi.org/10.1002/2016JE005009.

Bagenal, F., Adriani, A., Allegrini, F., Bolton, S.J., Bonfond, B., Bunce, E.J., et al., 2017. Magnetospheric science objectives of the Juno mission. Space Sci. Rev. https://doi.org/10.1007/s11214-014-0036-8.

Becker, H.N., Alexander, J.W., Adriani, A., et al., 2017. The Juno radiation monitoring (RM) investigation. Space Sci. Rev. 213, 507–545. https://doi.org/10.1007/s11214-017-0345-9.

Benn, M., Jorgensen, J.L., Denver, T., Brauer, P., Jorgensen, P.S., Andersen, A.C., et al., 2017. Observations of interplanetary dust by the Juno magnetometer investigation. Geophys. Res. Lett. 44. https://doi.org/10.1002/2017GL073186.

Bolton, S.J., Lunine, J., Stevenson, D., et al., 2017. The Juno mission. Space Sci. Rev. 213, 5–37. https://doi.org/10.1007/s11214-017-0429-6.

Bonfond, B., Hess, S., Bagenal, F., Gérard, J.C., Grodent, D., Radioti, A., Gustin, J., Clarke, J.T., 2013. The multiple spots of the Ganymede auroral footprint. Geophys. Res. Lett. 40, 4977–4981. https://doi.org/10.1002/grl.50989.

Bonfond, B., Saur, J., Grodent, D., Badman, S.V., Bisikalo, D., Shematovich, V., Gérard, J.C., Radioti, A., 2017. The tails of the satellite auroral footprints at Jupiter. J. Geophys. Res.: Space Phys. 122, 7985–7996. https://doi.org/10.1002/2017JA024370.

Caudal, G., 1986. A self-consistent model of Jupiter's magnetodisc including the effects of centrifugal force and pressure. J. Geophys. Res. 91 (A4), 4201. https://doi.org/10.1029/ja091ia04p04201.

Chew, G.F., Goldberger, M., Low, F., 1955. The individual particle equations of motion in the adiabatic approximation. Los Alamos Sci. Lab. Rept. LA–2055, chapter T–759.

Connerney, J.E.P., Benn, M., Bjarno, J.B., et al., 2017. The Juno magnetic field investigation. Space Sci. Rev. 213, 39–138. https://doi.org/10.1007/s11214-017-0334-z.

Connerney, J.E.P., Kotsiaros, S., Oliversen, R.J., Espley, J.R., Joergensen, J.L., Joergensen, P.S., Merayo, J.M.G., Herceg, M., Bloxham, J., Moore, K.M., Bolton, S.J., Levin, S.M., 2018. A new model of Jupiter's magnetic field from Juno's first nine orbits. Geophys. Res. Lett. 45, 2590–2596. https://doi.org/10.1002/2018GL077312.

Connerney, J.E.P., Timmins, S., Herceg, M., Jørgensen, J.L., 2020. A jovian magnetodisc model for the Juno Era. J. Geophys. Res.: Space Phys. 125 (10), 11 e2020JA028138.

Frank, L.A., Patterson, W.R., Ackerson, K.L., Bolton, S.J., 1997. Low-energy electron measurements at Ganymede with Galileo spacecraft: probe of the magnetic topology. Geophys. Res. Lett. 24, 2159–2162.

Gershman, D.J., Connerney, J.E., Kotsiaros, S., DiBraccio, G.A., Martos, Y.M., Viñas, A.F., et al., 2019. Alfvénic fluctuations associated with Jupiter's auroral emissions. Geophys. Res. Lett. 46 (13), 7157–7165.

Guio, Patrick, Staniland, Ned, Achilleos, Nicholas, Arridge, C., 2020. Trapped particle motion in Magnetodisk fields. J. Geophys. Res.: Space Phys. 125. https://doi.org/10.1029/2020JA027827.

Gurnet, D.A., Kurth, W.S., Roux, A., Bolton, S.J., 1996. Evidence for a magnetosphere at Ganymede from plasma-wave observation by the Galileo spacecraft. Nature 384, 535.

Herceg, Jørgensen, M.J.L., Merayo, J.M.G., Denver, T., Jørgensen, P.S., Benn, M., Kotsiaros, S., Connerney, J.E.P., 2021. Supplementary material for Energetic Electron Lensing Caused by Ganymede's Magnetic Field. https://doi.org/10.5281/zenodo.5503852. Zenodo.

Jorgensen, J.L., Benn, M., Connerney, J.E.P., Denver, T., Jorgensen, P.S., Andersen, A.C., Bolton, S.J., 2020. Distribution of interplanetary dust detected by the Juno spacecraft and its contribution to the Zodiacal Light. J. Geophys. Res.: Planets 125, e2020JE006509. https://doi.org/10.1029/2020JE006509.

Kivelson, M.G., K.K. Khurana, C.T. Russel, R.J. Walker, J. Warnecke, F.V. Coroniti, C. Plolanskey, D.J. Southwood, G. Shubert, Discovery of Ganymede's magnetic field by the Galileo spacecraft, Nature, 384, p. 537.

Kivelson, M.G., Khurana, K.K., Coroniti, F.V., et al., 1997. The magnetic field and magnetosphere of Ganymede. Geophys. Res. Lett. 24, 2155–2158.

Kivelson, M.G., Khurana, K., Volwerk, M., 2002. The permanent and inductive magnetic moments of Ganymede. Icarus 157, 507–522.

Kotsiaros, S., Connerney, J.E.P., Clark, G., et al., 2019. Birkeland currents in Jupiter's magnetosphere observed by the polar-orbiting Juno spacecraft. Nat. Astron. 3, 904–909. https://doi.org/10.1038/s41550-019-0819-7.

Kruskal, M., 1958. The Gyration of a Charged Particle. Project Matterhorn Rept. PM–S–33 (NYO7903), Princeton University. March.

Liuzzo, L., Poppe, A.R., Paranicas, C., Nénon, Q., Fatemi, S., Simon, S., 2020. Variability in the energetic electron bombardment of Ganymede. J. Geophys. Res.: Space Phys. 125, e2020JA028347. https://doi.org/10.1029/2020JA028347.

Louis, C.K., Louarn, P., Allegrini, F., Kurth, W.S., Szalay, J.R., 2020. Ganymede–induced decametric radio emission: in situ observations and measurements by Juno. Geophys. Res. Lett. 47 (20) e2020GL090021.

Mauk, B.H., McEntire, R.W., Williams, D.J., Lagg, A., Roelof, E.C., Krimigis, S.M., Armstrong, T.P., Fritz, T.A., Lanzerotti, L.J., Roederer, J.G., Wilken, B., 1998. Galileo-measured depletion of near-Io hot ring current plasmas since the Voyager epoch. J. Geophys. Res.: Space Phys. 103, 4715–4722. https://doi.org/10.1029/97ja02343.

Mauk, B.H., Clark, G., Gladstone, G.R., Kotsiaros, S., Adriani, A., Allegrini, F., et al., 2020. Energetic particles and acceleration regions over Jupiter's polar cap and main aurora; a broad overview. J. Geophys. Res.: Space Phys. 125. https://doi.org/10.1029/2019JA027699.

Mauk, B.H., Allegrini, F., Bagenal, F., Bolton, S.J., Clark, G., Connerney, J.E.P., Gershman, D.J., Haggerty, D.K., Hue, V., Imai, M., Kollmann, P., Kurth, W.S., N\'enon, Q., Paranicas, C.P., Rymer, A.M., Smith, H.T., Sulaiman, A.H., 2022. Loss of energetic ions comprising the ring current populations of Jupiter's Middle and inner magnetosphere. J. Geophys. Res. 127 (5), e30293. https://doi.org/10.1029/2022JA030293McIlwain.

McIlwain, C.E., 1961. Coordinates for mapping the distribution of magnetically trapped particles. J. Geophys. Res. https://doi.org/10.1029/JZ066i011p03681.

Mead, G.D., Hess, W.N., 1973. Jupiter's radiation belts and the sweeping effects of its satellites. J. Geophys. Res. 78, 2793.

Mogro-Campero, A., 1976. Absorption of Radiation Belt Particles by the Inner Satellites of Jupiter. In: Gehrels, T. (Ed.), Jupiter. University of Arizona Press, Tucson, p. 1190.

Mogro-Campero, A., Fillius, R.W., 1974. The radial diffusion coefficient of particle transport in the inner magnetosphere of Jupiter. Eos Trans. A GU 55, 1172.

Mogro-Campero, A., Fillius, R.W., 1976. The absorption of trapped particles by the inner satellites of Jupiter and the radial diffusion coefficient of particle transport. J. Geophys. Res. 81, 128.

Northrop, T.G., 1966. Adiabatic theory of charged particle motion. In: McCormac, B.M. (Ed.), Radiation Trapped in the Earth's Magnetic Field, Astrophysics and Space Science Library (A Series of Books on the Developments of Space Science and of General Geophysics and Astrophysics Published in Connection with the *Journal Space Science Reviews*), vol. 5. Springer, Dordrecht. https://doi.org/10.1007/978-94-010-3553-8_3.

Öztürk, M.K., 2012. Trajectories of charged particles trapped in Earth's magnetic field. Am. J. Phys. 80, 420. https://doi.org/10.1119/1.3684537.

Paranicas, Cris, Cheng, Andrew F., 1997. A model of satellite Microsignatures for saturn. Icarus 125 (2), 380–396. ISSN 0019-1035.

Paranicas, C., Paterson, W.R., Cheng, A.F., et al., 1999. Energetic particle observations near Ganymede. J. Geophys. Res. 104, 17459–17470.

Paranicas, C., Mauk, B., Haggerty, D., Clark, G., Kollmann, P., Rymer, A., Szalay, Jamey, Ranquist, D., Bagenal, F., Levin, S., Connerney, J., Bolton, Scott, 2017. Radiation near jupiter detected by Juno/JEDI during PJ1 and PJ3: high-latitude radiation environment. Geophys. Res. Lett. 44. https://doi.org/10.1002/2017GL072600.

Roussos, E., Jones, G.H., Krupp, N., Paranicas, C., Mitchell, D.G., Lagg, A., Woch, J., Motschmann, U., Krimigis, S.M., Dougherty, M.K., 2007. Electron microdiffusion in the Saturnian radiation belts: cassini MIMI/LEMMS observations of energetic electron absorption by the icy moons. J. Geophys. Res. 112, A06214. https://doi.org/10.1029/2006JA012027.

Roussos, R., Andriopoulou, M., Krupp, N., Kotova, A., Paranicas, C., Krimigis, S.M., Mitchell, D.G., 2013. Numerical simulation of energetic electron microsignature drifts at Saturn: Methods and applications. Icarus 226 (2), 1595–1611. https://doi.org/10.1016/j.icarus.2013.08.023.

Roussos, E., Krupp, N., Kollmann, P., Paranicas, C., Mitchell, D.G., Krimigis, S.M., Andriopoulou, M., 2016. Evidence for dust-driven, radial plasma transport in Saturn's inner radiation belts. Icarus 274, 272–283.

Selesnick, R.S., 1993. Micro- and macro- signatures of energetic charged particles in planetary magnetospheres. Adv. Space Res. 13 (10), 221–230. ISSN 0273-1177.

Simpson, J.A., Hamilton, D.C., McKibben, R.B., A, 1974. Mogro-Campero, K. R. Pyle, and A. J. Tuzzolino, the protons and electrons trapped in the Jovian dipole magnetic field region and their interaction with Io. J. Geophys. Res. 79, 3522.

Sulaiman, A.H., Hospodarsky, G.B., Elliott, S.S., Kurth, W.S., Gurnett, D.A., Imai, M., Allegrini, F., Bonfond, B., Clark, G., Connerney, J.E.P., Ebert, R.W., 2020. Wave–particle interactions associated with Io's auroral footprint: evidence of Alfvén, ion cyclotron, and whistler modes. Geophys. Res. Lett. 47 (22) e2020GL088432.

Szalay, J.R., et al., 2020. Alfvénic acceleration sustains Ganymede's footprint tail aurora. Geophysics Research Letters 47, e86527. https://doi.org/10.1029/2019GL086527.

Thomsen, M.F., 1976. Determination of the electron diffusion coefficient from observed Jovian satellite sweep-up effects (abstract). Eos Trans. AGU 57, 316.

Thomsen, M.F., 1977. On Determining a Radial Diffusion Coefficient from the Observed Effects of Jupiter's Satellites. Ph.D. thesis, Univ. of Iowa, Iowa City.

Thomsen, M.F., Goertz, C.K., 1975. Satellite sweep-up effects at Jupiter. Eos Trans. AGU 56, 428.

Thomsen, M.F., Van Allen, J.A., 1980. Motion of trapped electrons and protons in Saturn's inner magnetosphere. Progress report. United States: N. p.

Thomsen, M.F., Goertz, C.K., Van Allen, J.A., 1977a. A determination of the L dependence of the radial diffusion coefficient for protons in Jupiter's inner magnetosphere. J. Geophys. Res. 82, 3655.

Thomsen, M.F., Goertz, C.K., Van Allen, J.A., 1977b. On determining magnetospheric diffusion coefficients from the observed effects of Jupiter's satellite Io. J. Geophys. Res. 82 (35), 5541–5550. https://doi.org/10.1029/ja082i035p05541.

Van Allen, J.A., Thomsen, M.F., Randall, B.A., 1980. The energetic charged particle absorption signature of Mimas. J. Geophys. Res. 85 (A11), 5709–5718. https://doi.org/10.1029/JA085iA11p05709.

Williams, D.J., Mauk, B.H., McEntire, R.W., 1997a. Energetic particle signatures at Ganymede:implications for Ganymede's magnetic field. Geophys. Res. Lett. 24, 2163, 1997.

Williams, D.J., Mauk, B.H., McEntire, R.W., 1997b. Trapped electron in Ganymede's magnetic field. Geophys. Res. Lett. 24, 2953–2956, 1997.